A new studded precast concrete sandwich wall with embedded glass-fiber-reinforced polymer channel sections: Part 2, finite element analysis and parametric studies

Akram Jawdhari and Amir Fam

- This paper presents the finite element analysis (FEA) modeling of precast concrete sandwich panels with glass-fiber-reinforced polymer channel sections used as shear connectors.
- The validity of the FEA models was confirmed with the results from the experimental testing performed in a previous related study.
- The effect of channel connector geometry, concrete compressive strength, and concrete wythe reinforcement ratio on the precast concrete sandwich panel stiffness, strength, and degree of composite action was investigated.
- The results indicate that adjustments can be made to the panel design that improve the thermal efficiency of the panel without compromising the structural performance.

PCI Journal (ISSN 0887-9672) V. 65, No. 4, July–August 2020.
PCI Journal is published bimonthly by the Precast/Prestressed Concrete Institute, 8770 W. Bryn Mawr Ave., Suite 1150, Chicago, IL 60631.

Concrete sandwich panels have been used in the construction industry for more than 50 years, typically for building envelopes.[1] They are commonly composed of outer and inner wythes made of reinforced or prestressed concrete with rigid insulation sandwiched between the wythes to provide maximum thermal insulation. Concrete sandwich panels can be structurally classified as either fully composite, partially composite, or noncomposite.[1–3] The distinction among these three types of panels is based on the amount of horizontal shear transferred from one concrete wythe to the other through shear connectors in the form of solid concrete regions, discrete ties, trusses, and mesh grids.[1,4–6] In noncomposite panels, the concrete wythes act independently because the connectors linking them have negligible shear resistance.[7] The wythes can both be structural, but commonly one of them resists the loads while the other functions as a protective layer for the insulation foam core and as an architectural facade. In the case of fully composite panels, the two wythes act as a single unit through properly designed shear connectors, which are able to resist all of the horizontal shear.[7]

Partially composite panels are the general case, in which the connectors do not transfer the full shear.[8] Although the design and analysis of fully composite and noncomposite panels are simple and straightforward using the principles of force equilibrium and strain compatibility, partially composite panels pose a challenge because of the complexity of behavior and uncertainty about the amount of shear transferred across the wythes. The degree of composite action

of concrete sandwich panels is generally quantified through experimental tests combined with simplified analysis.[7] Experimental tests, though expensive and time consuming, are still needed to confirm the effectiveness of new panel designs and validate the results of numerical methods.[2,5–10]

A number of analytical models have been developed to study the performance of partially composite concrete sandwich panels. Hamed[11] presented a theoretical model for concrete sandwich panels with a steel truss connector. The model uses the principles of equilibrium and constitutive material models and accounts for axial and bending rigidities, cracking of concrete wythes, shear and normal rigidities of insulation foam, and elastic flexibility of the connector. A parametric study was also presented on the effects of the diameter and inclination angle of the truss connector and the thickness of concrete wythes and insulation layer. In a later study, Hamed[12] used the previously mentioned analytical model to investigate concrete sandwich panels with a diagonal shear connector made of fiber-reinforced polymer (FRP) bars. The model presented in the later study incorporated several revisions since the earlier study, including tension stiffening of concrete and a nonlinear stress–strain relationship for concrete in compression, yielding of steel wythe reinforcement, and expected failure modes. Tomlinson and Fam[3,4] also developed theoretical models to predict the behavior of concrete sandwich panels connected by angled basalt-FRP bars under flexural loads[3] and axial loads.[4]

Finite element analysis (FEA) has become widely popular in the past few decades. If properly calibrated with test data, FEA can significantly reduce the time and cost of research projects compared with additional experimental testing. One of the early FEA studies on concrete sandwich panels is by Bush and Wu,[13] who used solid elements for concrete and insulation and truss elements for the connectors with a linear solution. The model resulted in a conservative prediction of the panels' strength and stiffness. Lee and Pessiki[14] developed an FEA element model for two- and three-wythe panels and incorporated prestressing effects. Hopkins[15] used the FEA software Abaqus to develop a nonlinear model for concrete sandwich panels connected by segmental FRP plates under blast loads. A concrete damage plasticity model was implemented to simulate the behavior of concrete in tension and compression. The FEA model by Henin et al.[16] used shell elements to model the concrete and insulation and bar elements for the connectors, but the models were only applicable to service load levels.

In this study, comprehensive nonlinear FEA models were developed for the new concrete sandwich panel design presented in the companion paper.[17] The models incorporated various material and geometric features, including concrete nonlinearity and crushing in compression, concrete cracking and stiffening in tension, interfacial laws for parts in contact (for example, concrete to glass-fiber-reinforced polymer [GFRP] channel, concrete to insulation, and insulation to GFRP channel interfaces), steel plasticity, failure of GFRP channel using the Hashin model,[18] and geometric nonlinearity and buckling failure. The models were verified against the experimental results in the companion paper and used in a parametric study to examine the effects of steel reinforcement ratio, the ratio between the unsupported depth of the channel (which is equal to the insulation thickness) and the channel web thickness d_w/t_w, the channel flange thickness t_f, and concrete compressive strength. The effects of introducing openings in the GFRP channel web to reduce thermal bridging were studied in terms of shape and size of the opening (for example, diameter D and clear spacing S of circular openings).

FEA model development

The FEA models were developed in Ansys APDL commercial software. The three-dimensional panel model consisted of the two reinforced concrete wythes, insulation layer, GFRP channel connector, and steel plates at the loading and support locations. Symmetry conditions were applicable in the longitudinal direction but not in the transverse direction due to the unsymmetrical shape of the GFRP connector. Hence, the model was generated for half of the panel length and the entire width (**Fig. 1**).

FEA mesh and boundary conditions

The concrete wythes were modeled using cubic elements with a maximum side length of 25 mm (1 in.) (Fig. 1). The maximum element length of the cubes was increased to 50 mm (2 in.) for the insulation layer because of its negligible structural stiffness and strength (Fig. 1). The GFRP channel was meshed with one shell element through the thickness and multiple elements in the other two directions, with a maximum element length of 10 mm (0.4 in.) (Fig. 1). The boundary conditions consisted of a roller restraint ($U_y = 0$) at the support and symmetry conditions at midspan for the half-length model. All nodes were restrained at the midspan section in the x direction ($U_x = 0$) (Fig. 1). Additional rotational restraints ($\theta_y = \theta_z = 0$) were applied to the channel section nodes at midspan because the channel was modeled with shell elements that had transitional and rotational degrees of freedom (DOFs). The applied load was modeled as nonzero vertical displacements (Fig. 1) to accurately capture the load history, including the decrease in load after local damage (for example, concrete crushing, FRP rupture, and debonding) and the postfailure response.

Element types

Multiple types of elements were used to model the different parts of the concrete sandwich panel (Fig. 1). These elements are summarized in this section.

SOLID65 The concrete wythes were modeled with the eight-node SOLID65 element available in the Ansys library. This element, whose nodes have three translational DOFs, has special features for modeling brittle materials such as concrete and soil. The element is capable of modeling concrete's

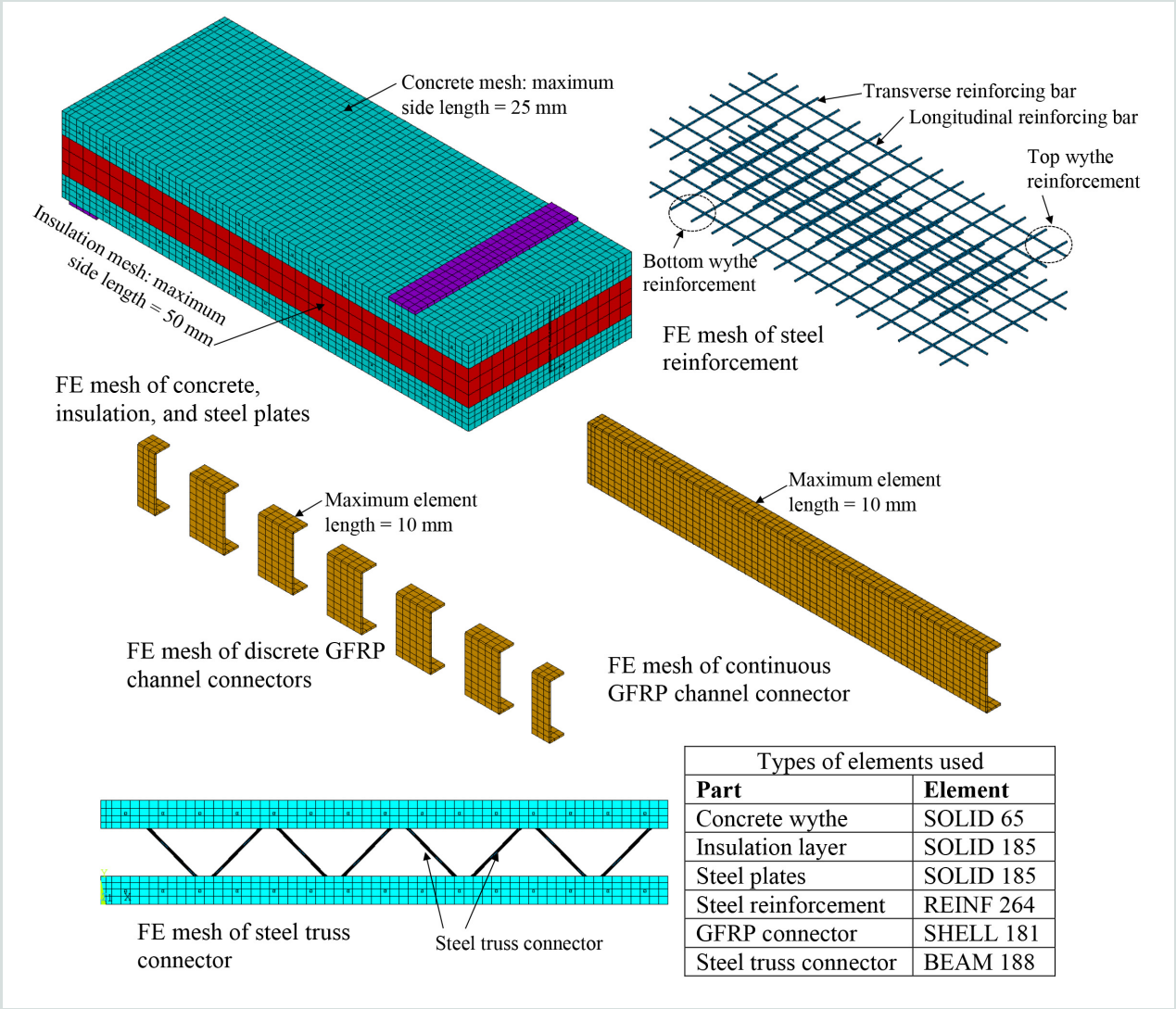

Types of elements used	
Part	**Element**
Concrete wythe	SOLID 65
Insulation layer	SOLID 185
Steel plates	SOLID 185
Steel reinforcement	REINF 264
GFRP connector	SHELL 181
Steel truss connector	BEAM 188

Figure 1. Finite element model. Note: FE = finite element; GFRP = glass-fiber-reinforced polymer. 1 mm = 0.0394 in.

nonlinear stress-strain response in compression, crushing, and cracking in three orthogonal directions and tension stiffening after cracking.

SOLID185 The insulation layer and steel plates at the support and loading locations were modeled with the eight-node SOLID185 element. Similar to the concrete element, SOLID185 nodes also have three translational DOFs in the x, y, and z axes. The element is capable of modeling nonlinear material stress-strain responses, plasticity, stress stiffening, and large deformations.

REINF264 The steel wire mesh used as longitudinal and transverse reinforcement for the concrete wythes was modeled with the REINF264 element. The element has two nodes, each with three translational DOFs, and is capable of modeling axial (tension, compression, or both) behavior only. Assigned to a base solid element, SOLID65 in this case, the nodes of REINF264 are coupled with the base element nodes, thus assuming that the slip between steel mesh and concrete is negligible.

SHELL181 The GFRP channel connector was modeled using a four-node shell element (SHELL181). The element has six DOFs, three translational and three rotational, and is suited for analyzing thin to moderately thick shell structures with large strain, rotation, deformation, and nonlinear material responses. In this study, a reduced integration option with hourglass control was activated to prevent inaccurate results associated with shell distortion.

BEAM188 For the reference panel with steel truss connector (specimen TR in the companion paper[17]), the truss was modeled using beam element BEAM188. The beam element is defined by two nodes, each having six DOFs, three translational and three rotational. The beam element was selected because

it includes bending and shear deformation effects, necessary for simulating the rigid truss connector and its dowel action of transferring horizontal shear. In addition, connector buckling and stability failures can be captured by activating the geometric nonlinearity algorithm.

CONTA173 For any surfaces in contact (for example, the GFRP channel with concrete), a surface-to-surface contact-target pair of elements was inserted to simulate the interfacial contact and sliding behavior. The contact element CONTA173 has four nodes and was placed on the surface containing softer material or finer FEA mesh, as recommended by Ansys. On the other surface, a companion target element, TARGE170, was placed. In addition to the contact-target pair, a bond-slip relation or cohesive zone model is needed to define the interface behavior in the normal and tangential directions. This is discussed in the following section.

Interfacial models

An interfacial relation, such as a bond-slip model or frictional law, is needed to model the contact-target elements. In the case of the concrete sandwich panels investigated here, three surfaces were found to be in contact:

- concrete and GFRP channel connector at the embedded part of the channel (interface 1)
- GFRP channel and insulation at the unsupported section of the channel web (interface 2)
- concrete and insulation (interface 3)

Interface 1 For the concrete-channel interface, a frictional contact model was used in the tangential direction. This model better relates to the interface, given its low bond strength of 0.28 MPa (0.04 ksi) and the large amount of slip recorded at the wythe ends, as determined experimentally in the companion paper.[17] The Mohr-Coulomb friction model available in Ansys was used for this interface and is defined as follows:

$$\tau = COHE + \mu \times N \quad (1)$$

where

τ = interface shear stress

$COHE$ = interface cohesion when stress $\sigma = 0$, which is the 0.28 MPa (0.04 ksi) bond strength measured from the push-off specimens

μ = coefficient of friction

N = normal contact pressure

A value of 0.2 was used for the friction coefficient μ of the GFRP section.[19] Sliding (tangential slip) between the two surfaces occurs when the shear stresses acting on the interface exceed τ in Eq. (1). In the direction normal to the concrete-channel interface, a full contact behavior (realized in Ansys by the no-separation option) was assumed because the channel was embedded in concrete, restraining the normal movement between the two parts.

Interface 2 The unsupported web of the channel could initially be in contact with the insulation, or the contact might develop after bending. Although the behavior of this interface was not expected to affect the behavior of the panel, the interface contact was also modeled. A frictionless contact was assumed, which allows the contacting surfaces to freely slide relative to each other but not interpenetrate normally. The *COHE* and μ parameters were set to zero.

Interface 3 The interface between concrete and insulation was not expected to develop any shear stresses because the insulation layer was wrapped with a bond-breaking sheet to prevent insulation adhesion and friction bond. Therefore, a frictionless contact, similar to the one used at interface 2, was also used for the concrete-insulation interface.

Material properties

Concrete wythes A nonlinear uniaxial stress-strain model proposed by Kent and Park[20] was used to represent the concrete compressive behavior (**Fig. 2**). The following mathematical expressions define the concrete model:

$$f_c = f_c'\left[2\left(\frac{\varepsilon}{\varepsilon_0}\right) - \left(\frac{\varepsilon}{\varepsilon_0}\right)^2\right] \quad \text{for } 0 \le \varepsilon \le \varepsilon_0$$

$$f_c = f_c'\left[1 - Z\left(\varepsilon_c - \varepsilon_0\right)\right] \quad \text{for } \varepsilon > \varepsilon_0$$

where

f_c = compressive stress at any strain ε

f_c' = concrete compressive strength

ε = stress

ε_0 = strain at f_c', which can be expressed as $\varepsilon_0 = \frac{2f_c'}{E_c}$

Z = the slope of the linear descending portion of the stress-strain curve for concrete in compression

ε_c = concrete strain

E_c = concrete elastic modulus, calculated as $E_c = 4700\sqrt{f_c'}$ following the American Concrete Institute's *Building Code Requirements for Structural Concrete (ACI 318-14) and Commentary (ACI 318R-14)*.[21]

The slope Z of the linear descending portion in the graph labeled "Concrete in Compression" in Fig. 2 is determined as follows for unconfined concrete:

$$Z = \frac{0.5}{\varepsilon_{50u} - \varepsilon_0}$$

where

ε_{50u} = strain at $f_c = 0.5f'_c$, which can be expressed as

$$\varepsilon_{50u} = \frac{30 + 0.002f'_c}{f'_c - 1000}$$

The concrete tensile stress-strain response was modeled as linear elastic before cracking at a maximum tensile stress f_t of $0.56\sqrt{f'}$ as defined by ACI 318.[21] Tension-stiffening effects were modeled with a linear descending curve ending at a strain of $6\varepsilon_t$, where ε_t is the strain at f_t (Fig. 2). A value of 0.2 was used for the open and closed shear transfer coefficients.[22,23] The Poisson's ratio of concrete was assumed to be 0.2.[22,23]

Steel For the steel wire mesh, which was used as flexural reinforcement for the concrete wythes and the steel truss connector in the reference panel (specimen TR in the com-

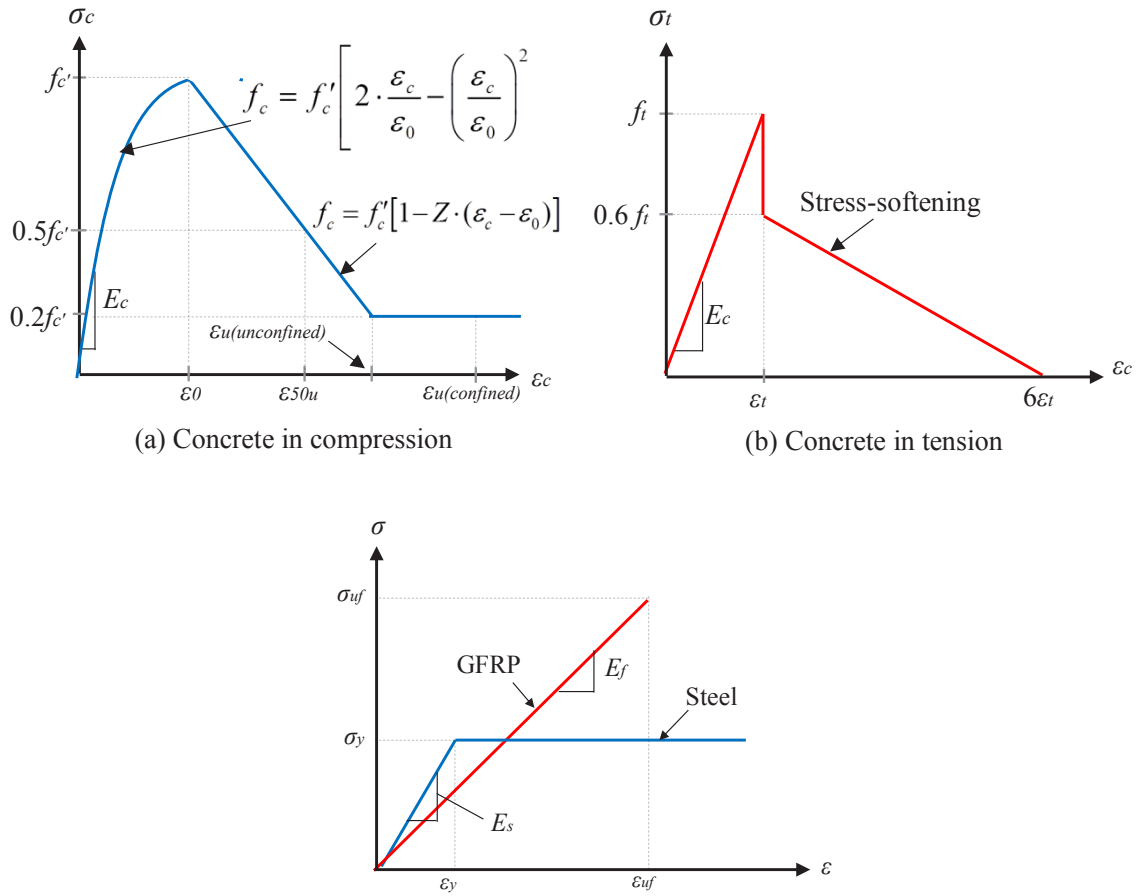

(a) Concrete in compression

(b) Concrete in tension

(c) Steel reinforcement and GFRP channel

Figure 2. Stress-strain models used in finite element analysis simulation. Note: E_c = concrete elastic modulus; E_f = elastic modulus of GFRP channel; E_s = elastic modulus of steel; f_c = concrete compressive stress at any strain; f'_c = concrete compressive strength; f_t = maximum concrete tensile stress; GFRP = glass-fiber-reinforced polymer; Z = slope of the linear descending portion of the stress–strain curve for concrete in compression; ε = strain; ε_c = concrete strain; ε_t = strain at the maximum concrete tensile stress; ε_u = ultimate concrete compressive strain; ε_{uf} = ultimate strain in the GFRP channel; ε_y = yield strain in the steel reinforcement; ε_0 = concrete compressive strain at f'_c; ε_{50u} = concrete compressive strain at f_c equal to $0.5f'_c$; σ = stress; σ_c = concrete compressive stress; σ_t = concrete tensile stress; σ_{uf} = ultimate stress of GFRP channel; σ_y = yield stress of steel reinforcement; σ = stress; σ_c = concrete compressive stress; σ_t = concrete tensile stress; σ_{uf} = ultimate stress of GFRP channel; σ_y = yield stress of steel reinforcement.

panion paper),[17] an elastic–perfectly plastic model was used (Fig. 2). The yield stress f_y was measured experimentally as 485 MPa (70.3 ksi). The elastic modulus E_s and Poisson's ratio ν for steel were assumed to be 200 GPa (29,000 ksi) and 0.3, respectively.

GFRP channel A linear elastic model was assumed for the GFRP channel (Fig. 2), whose properties in the direction parallel to fibers are different from the properties in other directions, also known as a specially orthotropic and transversely isotropic material.[24] **Table 1** lists the material properties for the channel section. In the experimental testing (presented in the companion paper),[17] failure in the channel was the governing failure mode of the panel, at which ultimate load was reached, followed by a sharp decrease in load.

To predict the panel's global behavior, including ultimate strength, accurate modeling of channel failure is needed. The composite damage model available in Ansys for FRP materials, known as the material property degradation method (MPDG), was used to simulate the failure mechanism of the GFRP channel. The model can predict five failure modes commonly observed in FRPs:

- fiber tension
- fiber compression
- matrix tension
- matrix compression
- interlaminar shear

Within the MPDG, a failure criterion defines the initiation of failure in any of the five failure modes when the stress or strain limit is reached. In this study, the Hashin failure criteria,[18] which are widely used in the literature,[25,26] have been adopted. **Table 2** lists the mathematical terms for defining the different FRP failure modes based on the Hashin criteria. In

Table 1. Mechanical properties of GFRP channel

Stiffness	Elastic modulus in fiber direction E_1, MPa	23*
	Elastic modulus in matrix direction E_2, MPa	9.32*
	Major Poisson's ratio v_{12}	0.33†
	Shear modulus G_{12}, MPa	2.93†
Strength	Tensile strength in fiber direction X^T, MPa	367*
	Compressive strength in fiber direction X^C, MPa	-186*
	Tensile strength in matrix direction Y^T, MPa	123*
	Compressive strength in matrix direction Y^C, MPa	-103*
	In-plane shear strength S^L, MPa	39†

Note: 1 MPa = 0.145 ksi.

* Determined from experimental tests in the companion paper. In case two values were reported for the flange and web, the lowest value was used in modeling the entire channel section.

† Taken from the manufacturer.

Table 2. Fiber-reinforced polymer damage model for channel connector

FRP failure mode	Governing stress	Hashin failure criteria
Fiber tension failure	$\sigma_{11} \geq 0$	$= \left(\frac{\sigma_{11}}{X^T}\right)^2 + \left(\frac{\tau_{11}}{Z^L}\right)^2$
Fiber compression failure	$\sigma_{11} < 0$	$= -\frac{\sigma_{11}}{X^C}$
Matrix tension failure	$\sigma_{11} > 0$	$= \left(\frac{\sigma_{22}}{Y^C}\right)^2 + \left(\frac{\tau_{12}}{S^L}\right)^2$
Matrix compression failure	$\sigma_{22} < 0$	$= \left(\frac{\sigma_{22}}{Y^C}\right)^2 + \left[\left(\frac{Y^C}{2S^L}\right)^2 - 1\right]\frac{\sigma_{22}}{Y^C} + \left(\frac{\tau_{12}}{S^L}\right)^2$
Fiber-matrix shear failure	$\sigma_{22} + \sigma_{33} > 0$	$= \left(\frac{\sigma_{11}}{X^T}\right)^2 + \left(\frac{\tau_{12}}{S^L}\right)^2$

Note: FRP = fiber-reinforced polymer; S^L = in-plane shear strength; X^C = compressive strength in fiber direction; X^T = tensile strength in fiber direction; Y^C = compressive strength in matrix direction; σ_{ij} = acting normal stress; τ_{ij} = acting shear stress.

addition to the failure criteria, a damage evolution criterion defines the material degradation after reaching the stress or strain limit. An instant stiffness reduction factor of 0.99 was applied to each affected mode and was selected based on previous work.[27]

Model verification

The load P compared with midspan deflection Δ plots presented the companion paper[17] compare the FEA prediction with the experimental results. In general, the FEA models showed reasonable agreement with the experimental results and were able to simulate the entire experimental panel behavior, including failure and postfailure stages. The FEA responses, however, were slightly stiffer for some of the tested panels.

The companion paper also compared the experimental and predicted maximum loads P_{max} for the five tested panels. The percentage difference between the predicted and experimental loads was 2% to 17%. The FEA simulations of the channel connector failure were an excellent match to the experimental results. By implementing the composite damage concept along with Hashin failure criteria, the models were able to accurately capture various channel failures, such as compression in top flange, shear in the web, and tension in the web and bottom flange. Furthermore, the models were also capable of simulating the slipping behavior at the three contact interfaces: concrete–channel, concrete–insulation, and insulation–channel.

Parametric study

The validated FEA model was used in a comprehensive parametric study using 70 individual model runs to examine the effects of several key parameters expected to affect the behavior of the concrete sandwich panel with a GFRP channel connector. The parameters studied were channel unsupported depth (insulation thickness)–to–web thickness ratio, channel flange thickness, concrete compressive strength, and

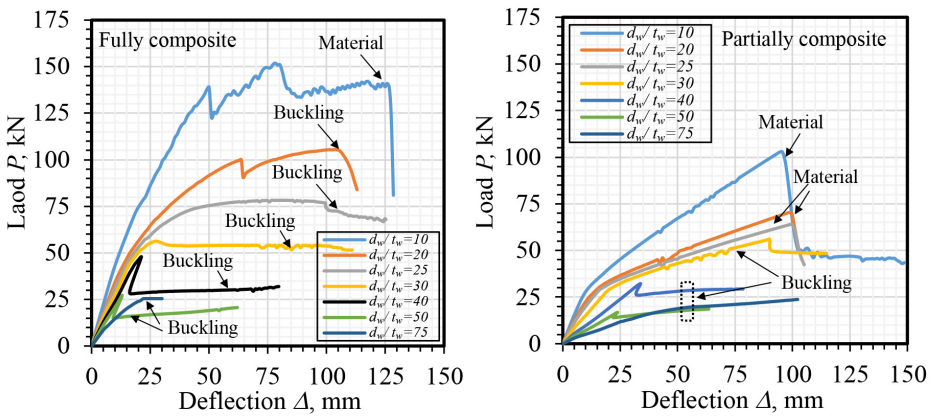

Load P compared with deflection Δ for fully and partially composite panels

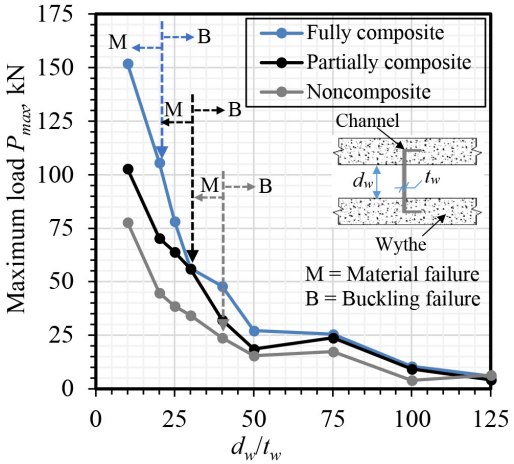

Figure 3. Effects of unsupported channel depth–to–web thickness ratio. Note: d_w = unsupported channel depth; t_w = channel web thickness. 1 mm = 0.0394 in.; 1 kN = 0.225 kip.

steel reinforcement ratio in the concrete wythes. The effect of introducing web openings in the GFRP web to minimize thermal bridging was also explored numerically, including variations of the shape of the opening and the diameter and spacing for circular openings. For some of these parameters, the analysis was performed for the two extreme conditions of fully composite and noncomposite panels, in addition to the actual case of partially composite panels.

Fully composite panels were idealized numerically by having the channel perfectly bonded to the concrete wythe (bonded contact), while still considering frictionless (unbonded) contact at the concrete–insulation and insulation–channel interfaces. On the other hand, the noncomposite panels were created by assuming that the concrete-channel interface was frictionless, similar to the other two interfaces.

Unsupported channel depth–to–thickness ratio d_w/t_w

The effects of the ratio of unsupported channel depth d_w to web thickness t_w on the panel behavior were studied by varying t_w from 1 to 13 mm (0.04 to 0.5 in.) such that d_w/t_w varied from 10 to 125. It is expected that increasing d_w/t_w will change the failure mode from material rupture to web buckling (stability failure). Local buckling is a commonly observed failure mode in thin-walled pultruded FRP sections with low modulus, such as GFRP.[28,29] To capture the stability failure in the FEA, a geometric nonlinearity algorithm was activated, which resulted in longer run times but more accurate results.

Figure 3 shows the load P compared with deflection Δ for the fully and partially composite panels with different d_w/t_w. Figure 4 also plots the maximum load P_{max} against d_w/t_w for the noncomposite, partially composite, and fully composite panels. Two failure modes were observed: material failure by compressive crushing in the channel flange and web and stability failure by channel web buckling. The transition from material to stability failure occurred at d_w/t_w equal to 20, 30, and 40 for the fully composite, partially composite, and noncomposite panels, respectively. As d_w/t_w increased, the strength and stiffness of the panel decreased (Fig. 3). Compared with material failure, the specimens with buckling failure (lower d_w/t_w) showed a more ductile behavior after reaching the peak load (Fig. 3). Figure 3 shows that for all three cases, P_{max} decreased sharply, by 82% on average, when d_w/t_w increased from 10 to 50. Beyond d_w/t_w equal to 50, P_{max} decreased at a much lower rate.

Figure 4 shows the material and stability failures in channel connectors with various d_w/t_w and degrees of composite action. In general, the material failure of compression crushing in the channel flange and web near midspan was identical for all observed cases and is shown by the red elements in Fig. 4 with a Hashin damage parameter of 1.0. However, the stability failure was variable, depending on d_w/t_w and degree of composite action. In some specimens, stability failure

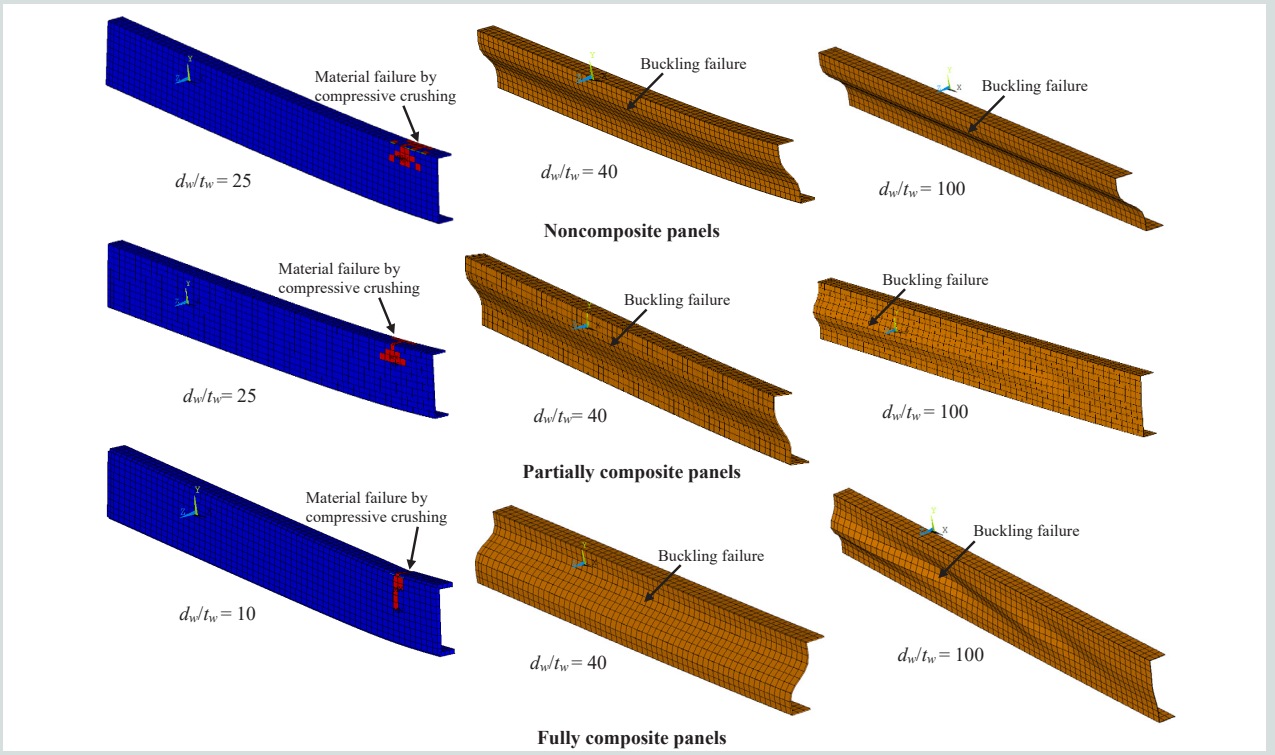

Figure 4. Channel material and stability failures for fully composite, partially composite, and noncomposite panels and different values of d_w/t_w. Note: d_w = unsupported channel depth; t_w = channel web thickness.

occurred throughout the entire channel length as a uniform second-order mode, as seen in Fig. 4 with d_w/t_w equal to 40, whereas in other specimens, buckling appeared randomly at parts of the channel, as seen in the second and third rows of Fig. 4 with d_w/t_w equal to 100. In those specimens, buckling occurred first near the supports, but as the load increased buckling approached the midspan region.

GFRP flange thickness t_f

Similar to the channel web thickness t_w investigated in the previous section, the effects of channel flange thickness t_f are explored in this section by varying the ratio of GFRP channel flange thickness–to–web thickness t_f/t_w from 0.25 to 2 for the partially composite panels. **Figure 5** displays the load-deflection responses for panels with different t_f/t_w and the relation between P_{max} and t_f/t_w. Increasing t_f/t_w resulted in an increase in the stiffness and ultimate load. However, the deflection at ultimate load remained constant at around 100 mm (4 in.), indicating that t_f has negligible effects on deformability. The panel failure was governed by the channel compressive crushing that occurred simultaneously in the top flange and web. A linear increase in P_{max} in relation to t_f/t_w is shown in Fig. 5, with P_{max} increasing by 25% when tf was doubled from $1.0t_w$, which was used in the experimental testing described in the companion paper,[17] to $2.0t_w$.

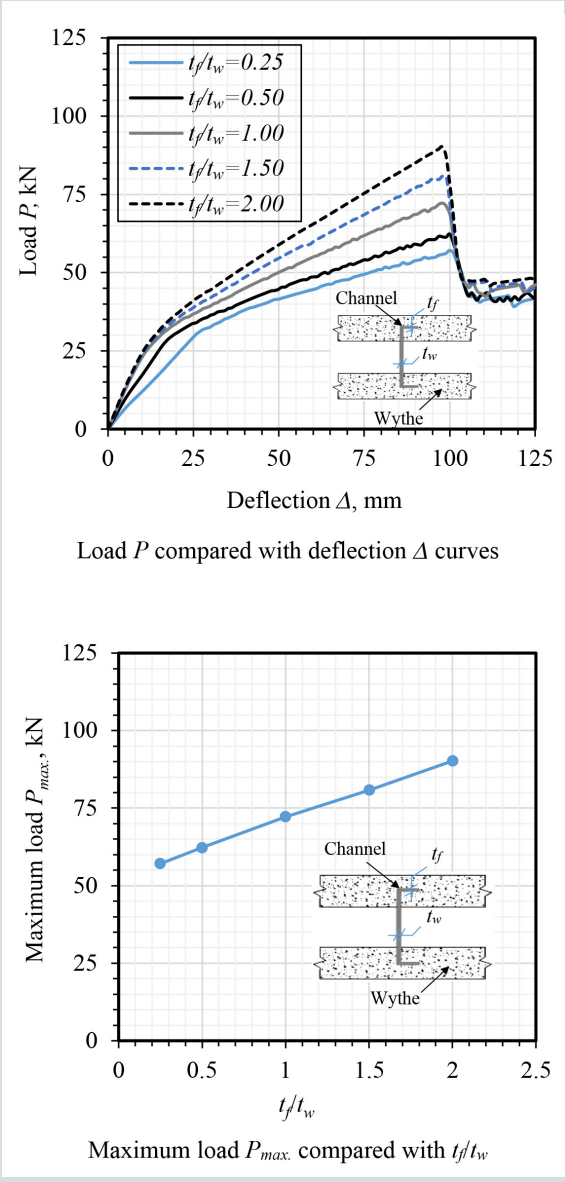

Figure 5. Channel material and stability failures for fully composite, partially composite, and noncomposite panels and different values of d_w/t_w. Note: d_w = unsupported channel depth; t_w = channel web thickness.

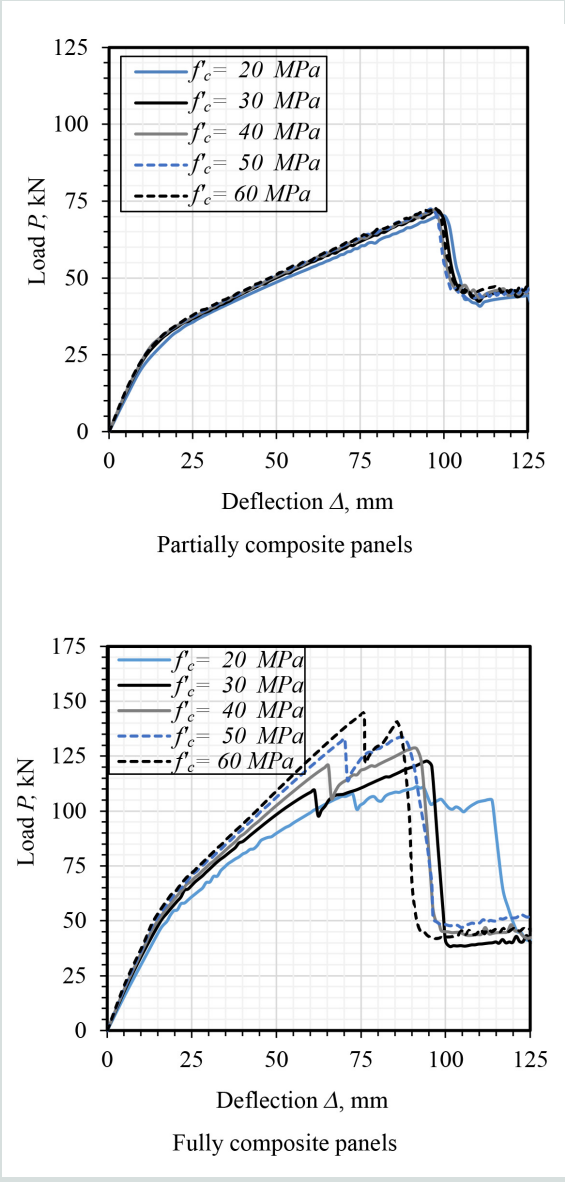

Figure 6. Load compared with deflection plots, with different concrete compressive strengths. Note: f'_c = concrete compressive strength. 1 mm = 0.0394 in.; 1 kN = 0.225 kip; 1 MPa = 0.145 ksi.

Concrete compressive strength f_c'

The concrete compressive strength f_c' varied from 20 to 60 MPa (2.9 to 8.7 ksi) for the partially and fully composite panels. For each f_c', new tensile and compressive stress-strain models were generated, according to the constitutive modeling presented earlier. **Figure 6** shows the load-deflection responses for the partially and fully composite panels. The top graph in Fig. 6 shows that the structural behavior of the partially composite panels was not largely affected by f_c'. On the other hand, for the fully composite panels, increasing f_c' led to an increase in the postyielding stiffness and maximum load P_{max}, which increased by 30% when f_c' increased from 20 to 60 MPa. To understand the difference in results between partially and fully composite cases, concrete flexural stresses at an arbitrary load P equal to 50 kN (11 kip), are plotted in Fig. 7. In the partially composite panel, tensile and compressive stresses occur in each wythe (the top graph in **Fig. 7**), indicating the presence of two neutral axes, one in each wythe. Both neutral axes are located very close to the wythe top edge, with a very small area in compression, and as such could not benefit from the increase in f_c'. For the fully composite panel, the wythes behave as a single unit, with only one neutral axis located close to the midheight of the top wythe (the bottom graph in Fig. 7). As such, the fully composite panel can gain some advantage from an increase in concrete compressive strength.

Steel reinforcement ratio ρ_s

The effects of steel reinforcement ratio ρ_s, which is the area of the steel reinforcement as a percentage of the wythe cross-sectional area, are investigated in this section by varying ρ_s from 0.1% to 2.5% for the partially composite panels. For precast concrete sandwich panels, design specifications[1,21] provide the minimum limit of ρ_s as equal to 0.1%, with no indications of

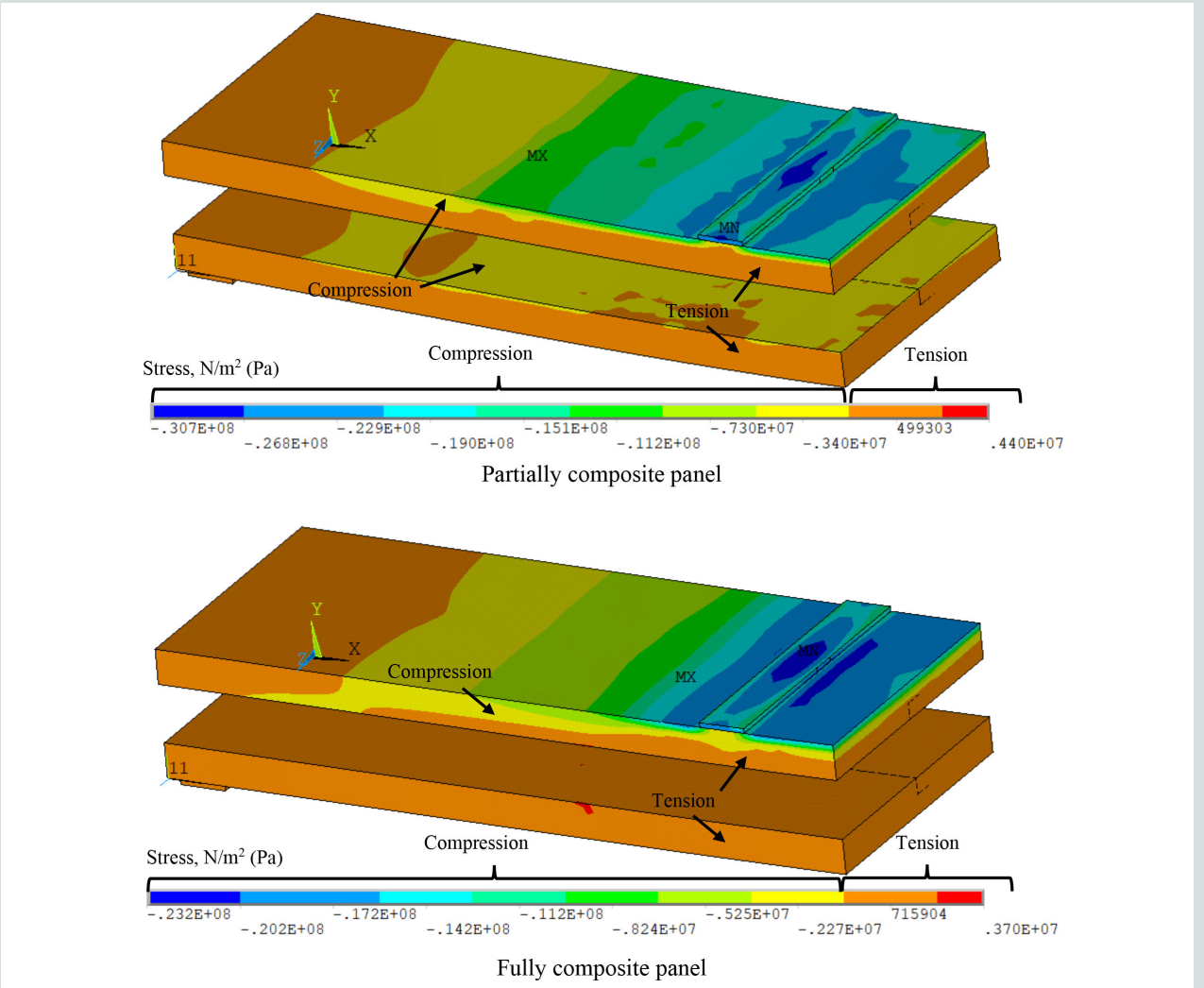

Figure 7. Concrete flexural stresses at P = 50 kN for wythes with f_c' = 60 MPa. Note: f_c' = concrete compressive strength; MN = minimum stress in contour; MX = maximum stress in contour; P = load. 1 kN = 0.225 kip; 1 N/m² = 1 Pa = 0.000145 psi; 1 MPa = 0.145 ksi.

a maximum value. In this parametric analysis, the reinforcement ratio was controlled by changing the diameter of the reinforcing bars while keeping the number of bars constant and equal to those in specimen TR in the experimental testing described in the companion paper.[17] **Figure 8** shows the load-deflection relationship for different ρ_s and the variation of P_{max} with ρ_s. Increasing ρ_s resulted in a tangible increase of stiffness and ultimate load of the panel. P_{max} increased linearly and increased by 13% when ρ_s was doubled from 1% to 2%.

Introducing web openings in the GRFP channel: Diameter of circular web openings

One of the desirable characteristics of concrete sandwich panels is their excellent thermal efficiency, which is achieved by using an insulation layer positioned between the outer and inner concrete layers to reduce thermal flow and minimize the cost of cooling and heating in buildings.[1–4,7–9] Shear connectors, though essential for the structural integrity of the panel, can reduce their thermal efficiency by creating thermal bridges.[2] The thermal resistance of concrete sandwich panels depends mainly on the connector material, size, and number.[30] GFRP has an inherently low thermal conductivity, averaging $1/60$ to $1/13$ that of steel.[30] However, increasing the cross-sectional area of the GFRP connector reduces thermal efficiency.[31,32]

This study explores the idea of introducing circular perforations in the web of the GFRP connector to minimize thermal bridging without sacrificing structural effectiveness. New FEA models were developed to examine the effect of varying the diameter of the circular opening D as a percentage of the unsupported channel depth d_w, with D/d_w ranging from 0 to 1.5 at an interval of 0.2. In all cases, the clear spacing between the openings S was kept constant at d_w and reduced to $0.5d_w$ between the last opening and channel edge.

The first three graphs in **Fig. 9** show the load-deflection relationships for panels with various D/d_w, including the noncomposite, partially composite, and fully composite cases. For partially composite and noncomposite panels, the effect of circular openings on the panel stiffness is generally very small for all values of D/d_w. On the other hand, increasing the hole diameter for the fully composite panel led to a decrease in stiffness (the graph labeled "Load compared with deflection for fully composite panel" in Fig. 9). The graph labeled "Maximum load compared with D/d_w" in Fig. 9 shows the relationship between P_{max} and D/d_w. The maximum load P_{max} remained unchanged from D/d_w equals 0 until 0.6 and 0.8 for the partially composite and noncomposite cases, respectively. Beyond these ratios, P_{max} decreased gradually. For the fully composite panel, P_{max} decreased by 16% initially when D/d_w increased from 0 to 0.4, then plateaued for D/d_w = 0.4 to 0.6 and decreased again by 19% for D/d_w = 0.6 to 1.0.

The material failure, indicated by the red elements, of the channel with various values of D/d_w is shown in **Fig. 10** for the three cases of composite action. Failure of the partially composite and noncomposite panels was by compressive crushing of channel flange and web, while for the fully composite case, the channel failed mainly by tensile rupture. As a design recommendation for the most realistic case of a partially composite panel, it is suggested that circular openings with a diameter not exceeding $0.6d_w$ (60% of unsupported channel depth) be provided at a clear spacing of d_w, which will enhance thermal efficiency while not causing significant degradation in structural performance.

Introducing web openings in the GFRP channel: Spacing of circular web openings

In addition to the web opening diameter D, the effects of clear spacing S between circular openings were examined for the optimal diameter D of $0.6d_w$ established in the previous section. S was varied as a ratio of the web opening

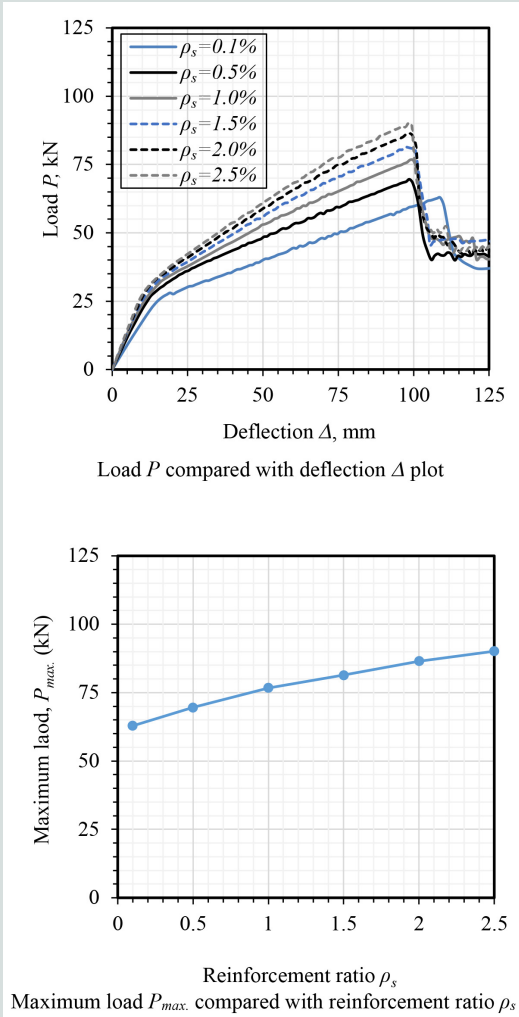

Figure 8. Effects of wythe flexural reinforcement ratio ρ_s. Note: 1 mm = 0.0394 in.; 1 kN = 0.225 kip.

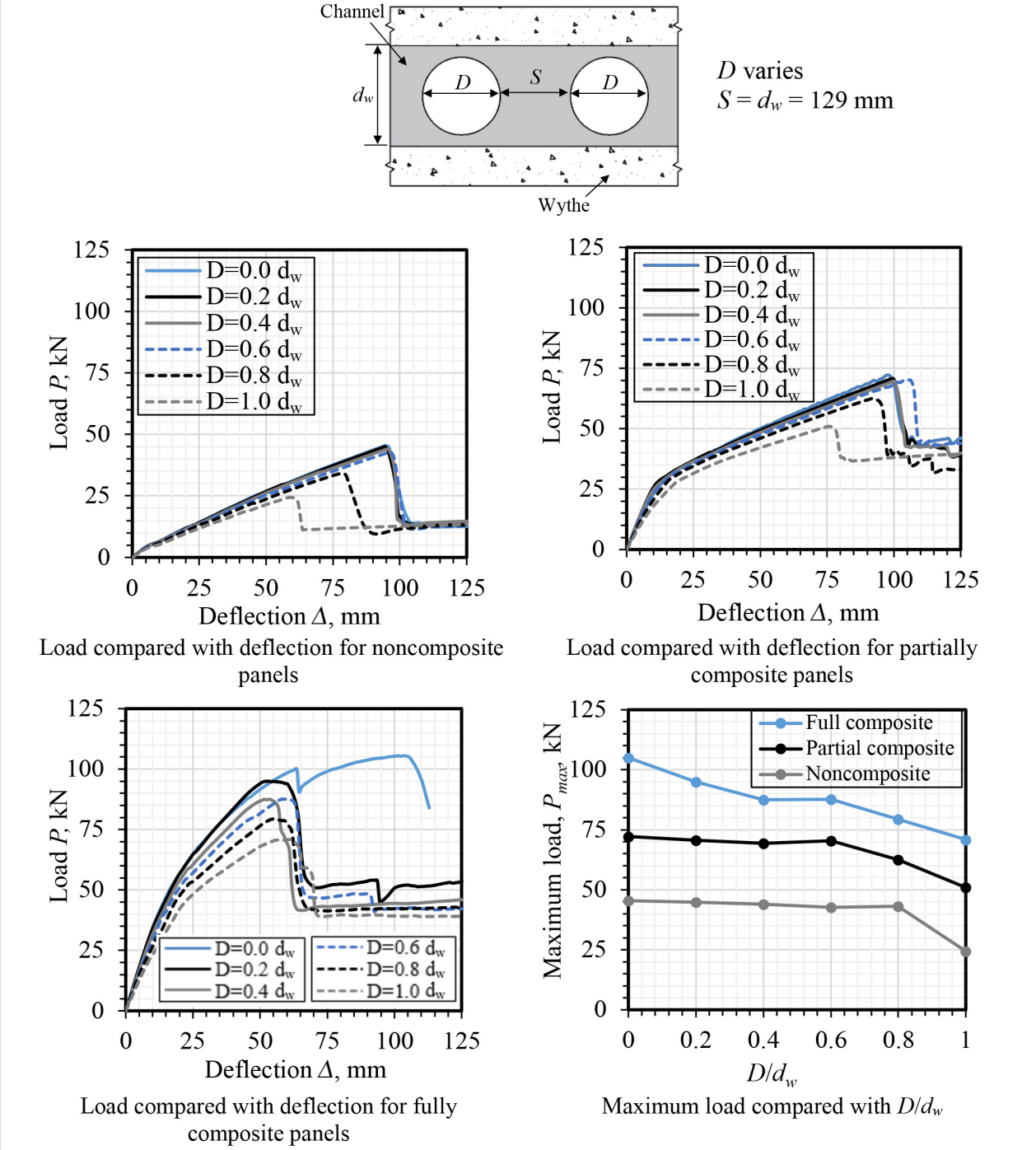

Figure 9. Effect of the diameter *D* of circular web opening in channel. Note: d_w = unsupported channel depth; *S* = clear spacing between circular web openings. 1 mm = 0.0394 in.; 1 kN = 0.225 kip.

diameter, with *S*/*D* ranging from 0.08 to 1.65 for the partially composite panels. **Figure 11** presents the load-deflection response and P_{max} compared with *S*/*D*. The figure shows that the global behavior was not affected when *S*/*D* was 0.84 or larger. At *S*/*D* less than 0.84, the maximum load decreased linearly and the stiffness also decreased due to the significant reduction in the channel web area. **Figure 12** shows the failure modes of the channel at different values of *S*/*D*. For *S*/*D* less than 0.84, channel failure occurred by shear between the openings. As *S*/*D* was increased beyond 0.84, shear failure was eliminated and compressive crushing of the flange and web governed at a higher load. Based on the anal-

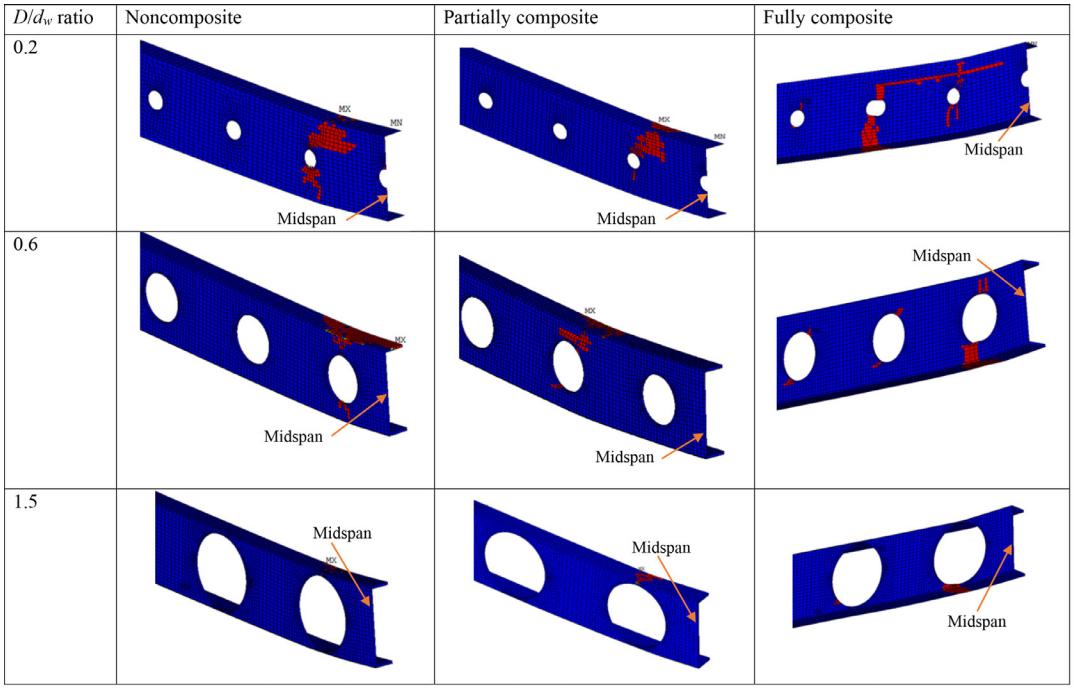

Figure 10. Failure in channels with different diameter D of circular web opening and different composite degrees. Note: Red elements indicate a Hashin parameter of 1.0 (failure). d_w = unsupported channel depth; MN = minimum stress in contour; MX = maximum stress in contour.

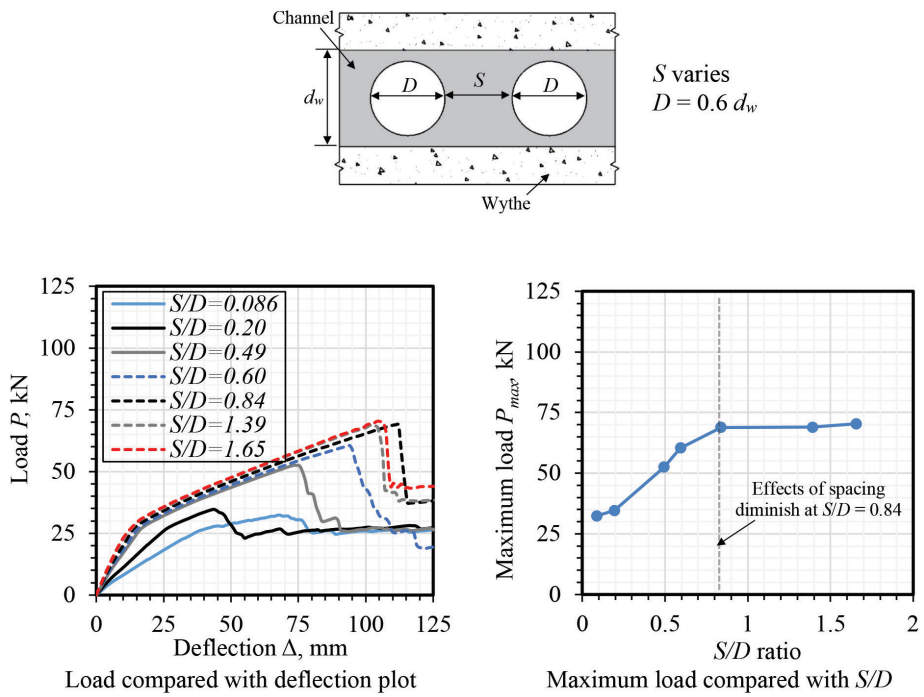

Figure 11. Effect of the clear spacing S of circular web opening of $0.6d_w$ diameter. Note: d_w = unsupported channel depth; D = diameter of circular web opening. 1 mm = 0.0394 in.; 1 kN = 0.225 kip.

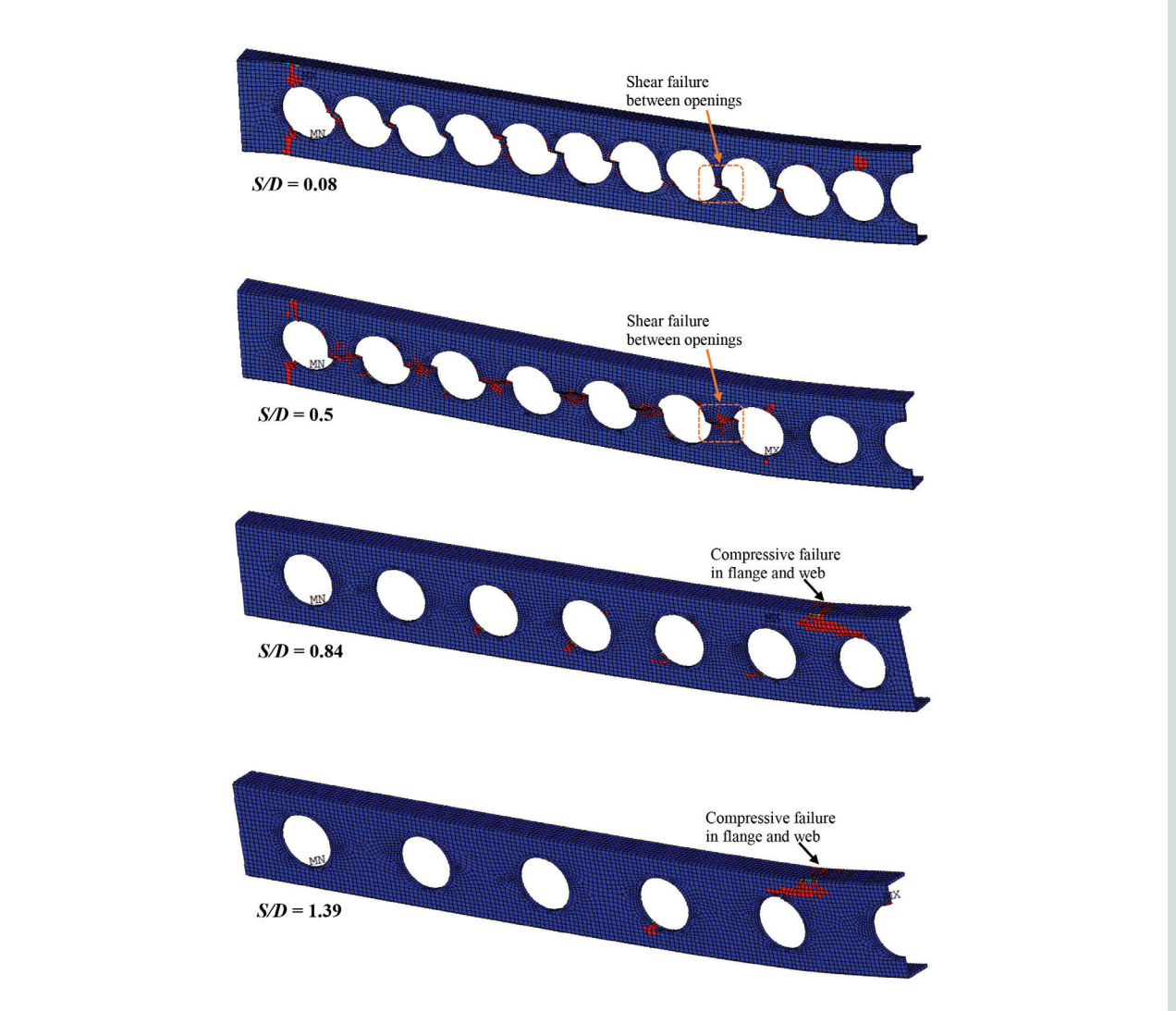

Figure 12. Failure in channels with different clear spacing *S* of circular web opening. Note: Red elements indicate a Hashin parameter of 1.0 (failure). *D* = diameter of circular web opening; MN = minimum stress in contour; MX = maximum stress in contour.

ysis, providing circular holes in the web with a maximum diameter of 0.6 times the unsupported channel depth (equal to the insulation thickness) and with a clear spacing not less than 0.84 times the hole diameter is recommended. This will ensure a panel strength equivalent to that of a panel with an unperforated GFRP channel.

Introducing web openings in the GFRP channel: Shape of the openings

Different geometries of web opening are discussed in this section, namely circular, diamond, hexagonal, and square. For all four geometries, the area of the hole was kept constant and equal to the area of the optimal circular opening established earlier with D/d_w of 0.6. The number of holes was also kept the same for all shapes. **Figure 13** shows the load-deflection responses for all four panels. The figure shows that the stiffness of the panel was not significantly affected by the opening shape. The maximum load P_{max}, however, was greatly affected by the opening shape.

The circular opening provided the highest load, at P_{max} = 70.4 kN (15.8 kip), followed by the diamond shape at P_{max} = 59.9 kN (13.5 kip) (or 85% of the circular hole panel), followed by the hexagonal shape at P_{max} = 55.9 kN (12.6 kip) (or 79% of the circular hole panel), and then by the square shape at P_{max} = 54.7 kN (12.3 kip) (or 77% of the circular hole panel).

Figure 14 displays the failure modes for channels with the four examined shapes. In the channel with circular openings, failure was by flange and web compressive crushing near the midspan section. For the channels with hexagonal and square openings, similar compressive failures occurred, but the failures were farther away from midspan. For the channel with diamond-shaped openings, failure was by shear between the openings.

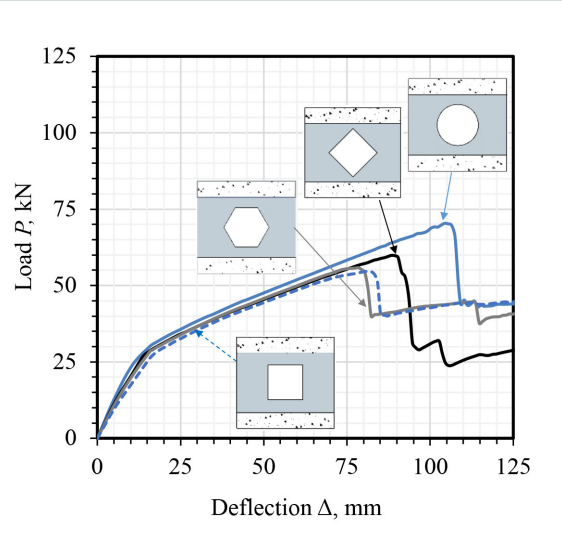

Figure 13. Plots of load P compared with deflection Δ for different shapes of channel web opening. Note: 1 mm = 0.0394 in.; 1 kN = 0.225 kip.

Assessment of degree of composite action

The previous sections assessed the effect of a number of parameters on the strength, stiffness, and failure mode of the concrete sandwich panel. In this section, the effects of selected parameters on the degree of composite action k are assessed. The degree of composite action was calculated from the following equation using the load method:[5]

$$k = \frac{P_{max}(\text{partial}) - P_{max}(\text{NC})}{P_{max}(\text{FC}) - P_{max}(\text{NC})} \times 100$$

where

P_{max}(partial) = maximum load from the FEA models for the partially composite panel

P_{max}(NC) = maximum load from the FEA models for the noncomposite case

P_{max}(FC) = maximum load from the FEA models for the fully composite case

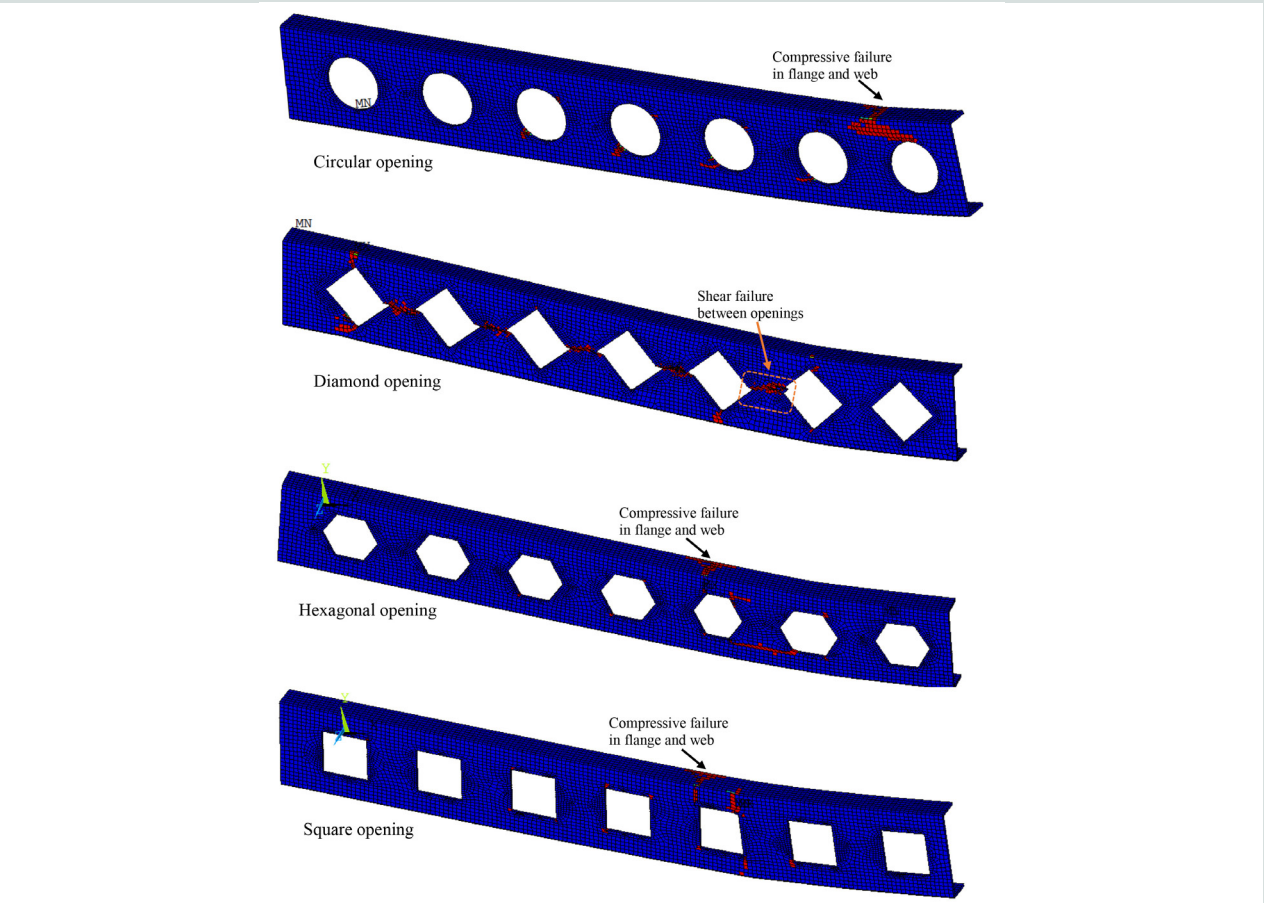

Figure 14. Failure in channels with different shapes of web opening. Note: Red elements indicate a Hashin parameter of 1.0 (failure). MN = minimum stress in contour; MX = maximum stress in contour.

Figure 15 shows the variation of k when two parameters are varied: the unsupported channel depth–to–thickness ratio d_w/t_w varying from 10 to 100 and the diameter of web opening–to–unsupported channel depth ratio D/d_w varying from 0 to 1. For d_w/t_w, k increased from 34% to 99% when d_w/t_w increased from 10 to 30. The degree of composite action decreased to k = 26% when d_w/t_w increased from 30 to 50 and then increased to an average k of 80% for d_w/t_w greater than 504. This inconsistent variation in k is likely due to the transition of the channel failure mode from material rupture to stability failure, which occurs at different values of d_w/t_w for the fully composite, partially composite, and noncomposite panels (Fig. 3). Even the stability failure was also somewhat inconsistent, occurring at local regions in some cases or spread through the entire channel in other cases (Fig. 5). The bottom graph in Fig. 16 shows that k seems to vary by a small amount, from k equals 45% to k equals 61%, as D/d_w increases from 0 to 0.6 and then decreases slightly at higher values of D/d_w. This variation is because the critical value of D/d_w is different for the partially composite and noncomposite cases (Fig. 9).

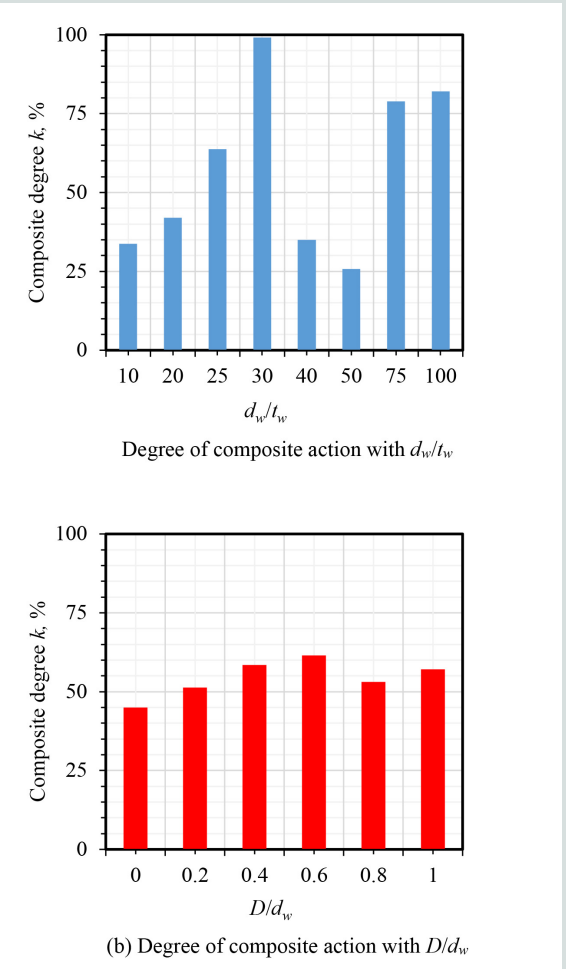

Figure 15. Variation of the degree of composite action k with d_w/t_w and D/d_w ratios. Note: D = diameter of circular web opening; d_w = unsupported channel depth; t_w = channel web thickness.

Conclusion

This study presents comprehensive FEA models developed to study the structural behavior of concrete sandwich panels with connectors made of a commercially available C-shaped GFRP channel section. The models included various features, such as concrete nonlinear response in compression, tension stiffening, cracking and crushing failures, Hashin failure criteria of the GFRP channel, interfacial modeling of different parts in contact, geometric nonlinearity, and stability failure of the channel. The models were validated using the experimental results reported in the companion paper, and very good agreements were observed. A comprehensive parametric study was carried out to examine the effects of several key parameters. Based on the results obtained, the following conclusions are drawn:

- For a given unsupported channel depth d_w (equal to the insulation thickness), reducing the web thickness of the channel section t_w reduced flexural strength and stiffness of the panel. Increasing d_w/t_w from 10 to 50 resulted in a sharp reduction in strength of 82% for the partially composite panel. The rate of reduction decreased thereafter as the increase of d_w/t_w from 50 to 100 resulted in a 9% strength reduction. The failure mode changed from material to stability failure of the channel section at d_w/t_w of 30.

- Increasing the flange thickness t_f of the GFRP channel relative to t_w resulted in an increase in flexural strength and stiffness of the partially composite panel. Increasing t_f/t_w from 1 to 2 increased the strength by 25%.

- Introducing holes in the web of the GFRP channel to reduce thermal bridging can be achieved without compromising the structural capacity of the panel. Circular, square, hexagonal, and diamond-shaped cuts of equal area were compared. The optimal cut shape that gave the highest flexural strength of the panel was the circular shape.

- Both the diameter D and clear spacing S of the circular holes in the GFRP channel web were varied independently. The optimal values of D/d_w and S/D for the partially composite panels that provide similar strength to that of the panels with an unperforated channel were 0.6 and 0.83, respectively. Smaller values of S/D resulted in premature shear failure between the holes at a reduced strength.

- Increasing concrete compressive strength f_c' from 20 to 60 MPa (2.9 to 8.7 ksi) does not affect the behavior of a partially composite panel. For a fully composite panel, however, increasing f_c' led to an increase in the postyielding stiffness and maximum load P_{max}, which increased by 30% when f_c' increased from 20 MPa to 60 MPa.

- Doubling the wythe steel reinforcement ratio ρ_s from 1% to 2% resulted in a 13% increase in the flexural strength of the partially composite panel, whereas increasing the concrete compressive strength from 20 to 60 MPa (2.9 to 8.7 ksi) had an insignificant effect on flexural strength.

References

1. PCI Committee on Precast Concrete Sandwich Panels. 2011. "State of the Art of Precast/Prestressed Concrete Sandwich Wall Panels." *PCI Journal* 56 (2): 131–176.

2. Tomlinson, D., and A. Fam. 2015. "Flexural Behavior of Precast Concrete Sandwich Wall Panels with Basalt FRP and Steel Reinforcement." *PCI Journal* 60 (6): 51–71.

3. Tomlinson, D., and A. Fam. 2016. "Analytical Approach to Flexural Response of Partially Composite Insulated Concrete Sandwich Walls Used for Cladding." *Engineering Structures* 122: 251–266.

4. Tomlinson, D., and A. Fam. 2016. "Analysis and Parametric Study of Partially Composite Precast Concrete Sandwich Panels under Axial Loads." *Journal of Structural Engineering* 142 (10). https://doi.org/10.1061/(ASCE)ST.1943-541X.0001560.

5. Frankl, B. A., G. W. Lucier, T. K. Hassan, and S. H. Rizkalla. 2011. "Behavior of Precast, Prestressed Concrete Sandwich Wall Panels Reinforced with CFRP Shear Grid." *PCI Journal* 56 (2): 42–54.

6. Maximos, H. N., W. A. Pong, M. L. Tadros, and L. D. Martin. 2007. "Behavior and Design of Composite Precast Prestressed Concrete Sandwich Panels with NU-Tie." Final report, University of Nebraska–Lincoln.

7. Benayoune, A., A. A. Samad, D. N. Trikha, A. A. Abang Ali, and S. H. M. Ellinna. 2008. "Flexural Behavior of Pre-cast Concrete Sandwich Composite Panel—Experimental and Theoretical Investigations." *Construction and Building Materials* 22 (4): 580–592.

8. Tomlinson, D., and A. Fam. 2016. "Combined Loading Behavior of Basalt FRP–Reinforced Precast Concrete Insulated Partially-Composite Walls." *Journal of Composites for Construction* 20 (3). https://doi.org/10.1061/(ASCE)CC.1943-5614.0000611.

9. Einea, A., D. C. Salmon, M. K. Tadros, and T. Culp. 1994. "A New Structurally and Thermally Efficient Precast Sandwich Panel System." *PCI Journal* 39 (4): 90–101.

10. Pessiki, S., and A. Mlynarczyk. 2003. "Experimental Evaluation of the Composite Behavior of Precast Concrete Sandwich Wall Panels." *PCI Journal* 48 (2): 54–71.

11. Hamed, E. 2016. "Modeling, Analysis, and Behavior of Load-Carrying Precast Concrete Sandwich Panels." *Journal of Structural Engineering* 142 (7). https://doi.org/10.1061/(ASCE)ST.1943-541X.0001490.

12. Hamed, E. 2017. "Load-Carrying Capacity of Composite Precast Concrete Sandwich Panels with Diagonal Fiber-Reinforced-Polymer Bar Connectors." *PCI Journal* 62 (4): 34–44.

13. Bush, T. D., and Z. Wu. 1998. "Flexural Analysis of Prestressed Concrete Sandwich Panels with Truss Connectors." *PCI Journal* 43 (5): 76–86.

14. Lee, B., and S. Pessiki. 2007. "Design and Analysis of Precast, Prestressed Concrete Three-Wythe Sandwich Wall Panels." *PCI Journal* 52 (4): 70–83.

15. Hopkins, P. M. 2015. "Non-linear Finite Element Analysis of FRP-Precast Concrete Sandwich Panels." PhD thesis, University of Idaho, Moscow, ID.

16. Henin, E., G. Morcous, and M. K. Tadros. 2014. "Precast/Prestressed Concrete Sandwich Panels for Thermally Efficient Floor/Roof Applications." *Practice Periodical on Structural Design and Construction* 19 (3): 1–13.

17. Dutta, D., A. Jawdhari, and A. Fam. 2020. "A New Studded Precast Concrete Sandwich Wall with Embedded Glass-Fiber-Reinforced Polymer Channel Sections: Part 1, Experimental Study." *PCI Journal* 65 (3): 78–99.

18. Hashin, Z. 1980. "Failure Criteria for Unidirectional Fiber Composites." *Journal of Applied Mechanics* 47 (2): 329–334.

19. Goyal, R., A. Mukherjee, and S. Goyal. 2016. "An Investigation on Bond between FRP Stay-in-Place Formwork and Concrete." *Construction and Building Materials* 113: 741–751.

20. Kent, D. C, and R. Park. 1971. "Flexural Members with Confined Concrete." *Journal of the Structural Division* 97 (7): 1969–1990.

21. ACI (American Concrete Institute) Committee 318. 2014. *Building Code Requirements for Structural Concrete (ACI 318-14) and Commentary (ACI 318R-14)*. Farmington Hills, MI: ACI.

22. Hawileh, R., J. A. Abdalla, and M. Tanarslan. 2012. "Modeling of Nonlinear Response of R/C Shear Deficient T-Beam Subjected to Cyclic Loading." *Computers and Concrete* 10 (4): 413–428.

23. Jawdhari, A., and I. Harik. 2017. "Finite Element Analysis of RC Beams Strengthened in Flexure with CFRP Rod Panels." *Construction and Building Materials* 163: 751–766.

24. Kachlakev, D. I., T. H. Miller, S. Yim, K. Chansawat, and T. Potisuk. 2001. "Finite Element Modeling of Concrete Structures Strengthened with FRP Laminates." Final report FHWA-OR-RD-01-17, SPR 316, United States Department of Transportation, Federal Highway Administration, and Oregon Department of Transportation, Salem, OR.

25. Anyfantis, K. N., and N. G. Tsouvalis. 2012. "Post Buckling Progressive Failure Analysis of Composite Laminated Stiffened Panels." *Applied Composite Materials* 19 (3–4): 219–236. https://doi.org/10.1007/s10443-011-9191-1.

26. Bsisu, K., H. Hussein, and S. Sargand. 2017. "The Use of Hashin Damage Criteria, CFRP–Concrete Interface and Concrete Damage Plasticity Models in 3D Finite Element Modeling of Retrofitted Reinforced Concrete Beams with CFRP Sheets." *Arabian Journal for Science and Engineering* 42 (3): 1171–1184.

27. El-Sisi, A. E., H. M. El-Emam, H. A. Salim, and H. E. M. Sallam. 2015. "Efficient 3D Modeling of Damage in Composite Materials." *Journal of Composite Materials* 49 (7): 817–828.

28. Qiao, P., and G. Zou. 2003. "Local Buckling of Composite Fiber-Reinforced Plastic Wide-Flange Sections." *Journal of Structural Engineering* 129 (1): 125–129.

29. Liu, T. 2017. "Stability Behavior of Pultruded Glass-Fiber Reinforced Polymer I-Sections Subject to Flexure." PhD diss., University of Pittsburgh, Pittsburgh, PA.

30. Woltman, G., M. Noel, and A. Fam. 2017. "Experimental and Numerical Investigations of Thermal Properties of Insulated Concrete Sandwich Panels with Fiberglass Shear Connectors." *Energy and Buildings* 145: 22–31.

31. McCall, W. C. 1985. "Thermal Properties of Sandwich Panels." *Concrete International* 7 (1): 35–41.

32. Kosny, J., P. Childs, and A. Desjarlais. 2001. *Thermal Performance of Prefabricated Concrete Sandwich Wall Panels*. Oak Ridge, TN: Oak Ridge National Laboratory Buildings Technology Center.

Notation

$COHE$ = interface cohesion when the contact pressure is equal to 0

d_w = unsupported channel depth

D = diameter of the circular opening in the channel

E_1 = elastic modulus in fiber direction

E_2 = elastic modulus in matrix direction

E_c = concrete elastic modulus

E_f = elastic modulus of the GFRP channel

E_s = elastic modulus of steel

f_c = compressive stress at any strain

f_c' = concrete compressive strength

f_t = maximum concrete tensile stress

f_y = yield stress of steel reinforcement

G_{12} = shear modulus

k = degree of composite action

MN = minimum stress in contour

MX = maximum stress in contour

N = normal contact pressure

P = load

P_{max} = maximum load

P_{max}(FC) = maximum load from the FEA models for the fully composite case

P_{max}(NC) = maximum load from the FEA models for the noncomposite case

P_{max}(partial) = maximum load from the FEA models for the partially composite panel

S = clear spacing between the circular openings in the channel

S^L = in-plane shear strength

t_f = channel flange thickness

t_w = channel web thickness

U_x = displacement in the x direction

U_y = displacement in the y direction

X^C = compressive strength in fiber direction

X^T = tensile strength in fiber direction

Y^C = compressive strength in matrix direction

Y^T = tensile strength in matrix direction

Z = slope of the linear descending portion of the stress–strain curve for concrete in compression

Δ = midspan deflection

ε = strain

ε_0 = concrete compressive strain at f_c'

ε_{50u} = concrete compressive strain at fc equal to $0.5f_c'$

ε_c = concrete strain

ε_t = strain at the maximum concrete tensile stress

ε_u = ultimate concrete compressive strain

ε_{uf} = ultimate strain in the GFRP channel

ε_y = yield strain for the steel reinforcement

θ_y = rotation in the y direction

θ_z = rotation in the z direction

μ = coefficient of friction

ν = Poisson's ratio

ν_{12} = major Poisson's ratio

ρ_s = steel reinforcement ratio

σ = stress

σ_c = concrete compressive stress

σ_{ij} = acting normal stress

σ_t = concrete tensile stress

σ_{uf} = ultimate stress of GFRP channel

σ_y = yield stress of steel reinforcement

τ = interface shear stress

τ_{ij} = acting shear stress

About the authors

Akram Jawdhari is an adjunct faculty member and postdoctoral fellow in the Department of Civil Engineering at Queens University in Kingston, ON, Canada.

Amir Fam is a professor and associate dean for research and the Donald and Sarah Munro Chair in Engineering and Applied Science at Queens University.

Abstract

The effectiveness of glass-fiber-reinforced polymer (GFRP) pultruded channel sections as shear connectors in precast concrete sandwich walls has been demonstrated experimentally in the companion paper, "A New Studded Precast Concrete Sandwich Wall with Embedded Glass-Fiber-Reinforced Polymer Channel Sections: Part 1, Experimental Study." In this paper, three-dimensional nonlinear finite element analysis models of the previously tested panels are developed, verified, and used in a comprehensive parametric study. The models consider accurate constitutive laws for all materials, interfacial relations for different parts in contact, and different failure modes, including material and stability failure of GFRP channels.

The parametric study showed that increasing the ratio of the unsupported channel depth d_w to GFRP channel web thickness t_w led to a decrease in flexural strength and a shift in failure mode from material to stability failure of the GFRP connector, which occurs at d_w/t_w of 30 in the partially composite panel. When the channel flange thickness and the wythe steel reinforcement ratio were independently doubled, flexural strength increased by 25% and 13%, respectively. Concrete compressive strength had an insignificant effect on partially composite panel strength. To increase thermal efficiency without reducing structural effectiveness, the use of circular perforations in the GFRP channel web was explored. It was found that openings with a diameter D up to $0.6d_w$ and a clear spacing S not less than $0.84D$ can be effectively introduced without reducing the structural strength of the panel. Circular openings were shown to be more effective than diamond-shaped, hexagonal, or square openings.

Keywords

Composite action, finite element, GFRP, glass-fiber-reinforced polymer, sandwich panel, shear connector, stud, thermal efficiency.

Review policy

This paper was reviewed in accordance with the Precast/Prestressed Concrete Institute's peer-review process.

Reader comments

Please address any reader comments to *PCI Journal* editor-in-chief Tom Klemens at tklemens@pci.org or Precast/Prestressed Concrete Institute, c/o *PCI Journal*, 8770 W. Bryn Mawr Ave., Suite 1150, Chicago, IL 60606.